Anomalous Pressure Effect in Heteroacene Organic Field-Effect Transistors

K. Sakai,[1,*] Y. Okada,[1] S. Kitaoka,[1,2] J. Tsurumi,[1,2] Y. Ohishi,[3] A. Fujiwara,[3] K. Takimiya,[4,5] and J. Takeya[1,2,†]

[1]*ISIR, Osaka University, 8-1 Mihogaoka, Ibaraki, Osaka 567-0047, Japan*

[2]*Department of Applied Physics, Graduate School of Engineering, Osaka University, 1-1 Yamadaoka, Suita, Osaka 565-0871, Japan*

[3]*JASRI, SPring-8, 1-1-1 Kouto, Sayo-cho, Sayo-gun, Hyogo 679-5198, Japan*

[4]*Department of Applied Chemistry, Graduate School of Engineering, Hiroshima University, 1-4-1 Kagamiyama, Higashi-Hiroshima, Hiroshima 739-8527, Japan*

[5]*RIKEN, 2-1, Hirosawa, Wako, Saitama 351-0198, Japan*

(Received 12 October 2012; revised manuscript received 17 December 2012; published 28 February 2013)

Anomalous pressure dependent conductivity is revealed for heteroacene organic field-effect transistors of dinaphtho[2, 3-b:2′, 3′-f]thieno[3, 2-b]thiophene single crystals in the direction of a and b crystallographic axes. In contrast to the normal characteristics of a monotonic increase in mobility μ with the application of external hydrostatic pressure P in conductors, we found that the present organic semiconductor devices exhibit nonmonotonic and gigantic pressure dependence including an even negative pressure coefficient $d\mu/dP$. In combination with a structural analysis based on x-ray diffraction experiments under pressure, it is suggested that on-site molecular orientation and displacement peculiar in heteroacene molecules are responsible for the anomalous pressure effect.

DOI: 10.1103/PhysRevLett.110.096603 PACS numbers: 72.80.Le, 73.40.−c, 73.61.Ph

Solid-state assemblies of van der Waals bonded π-conjugated molecules, i.e., organic semiconductors, are of considerable interest both in scientific and industrial contexts. The pristine materials themselves are good insulators, so that electric conduction immediately turns on at the surfaces with the application of an electric field. The charge transport is composed of the consecutive charge transfer of π-electronic carriers between only weakly interacting molecular orbitals, which is essentially different from inorganic semiconductors with well-defined covalent networks for charges to propagate. Nevertheless, some of the organic semiconductor systems show moderate carrier mobility above 1 $\mathrm{cm}^2/\mathrm{V\,s}$ and the charge transport mechanism is consistent with band transport [1–4], but is on the verge of self-localization due to strong molecular fluctuation [5]. More microscopically, the peculiar shape of molecular orbitals in such compounds causes condensation into corresponding crystal structures in the ambient pressure as the result of the naïve balance between the mutually attracting London force and Coulomb repulsive force. Therefore, considerable impact is expected with the application of external pressure, not only by reducing the molecular distance but also by deforming the crystal structure due to freedom of the on-site molecular orientation. In addition to such scientific interest, studies on fundamental mechanical response are desired in the performance of organic field-effect transistors when subjected to bending force causing significant pressure, in the prospect of establishing a flexible and soft printed electronics industry.

Recently, we introduced a method of measuring the effect of hydrostatic pressure on charge carrier conductivity in organic semiconductor crystals, introducing the charge with the application of electric field at the semiconductor surfaces [6]. In addition to the measurement of common transfer characteristics of drain current I_D as a function of gate voltage V_G shown in former pioneering studies [7,8], we perform four-terminal conductivity measurements to exclude the extrinsic influence of the metal-to-semiconductor contact resistance. Moreover, we measured the Hall coefficient simultaneously to deduce the correct pressure coefficient, estimating the change in dielectric capacitance and thickness of the gate dielectric insulators, providing a route to study the so-called ''structure-property'' relations. We first applied the method to single crystal devices of rubrene which simply consists of only carbon and hydrogen atoms. The value of pressure coefficient $d\mu/dP$ turned out to be extremely high in comparison with that in inorganic systems. Here in the present studies, we found that the system of dinaphtho[2, 3-b:2′, 3′-f]thieno [3, 2-b]thiophene (DNTT) shows much more pronounced features of the pressure effect, characterized by far larger $d\mu/dP$ values whose sign can be even negative. The result cannot be understand by normal positive pressure effect due to an increasing charge-transfer rate with decreasing molecular distance without taking into account displacement, rotation, and other degrees of freedom originated from molecular structures. In combination with the measurement of anisotropic transport and the x-ray diffraction studies, we construct a plausible model of the pressure induced structural deformation.

In order to realize stable and reproducible measurement under high pressure, device structure and pressure cells were newly developed as reported previously [6]. In the present study, platelet-shaped single crystals of DNTT were employed as the channel material replacing rubrene. The DNTT single crystals are grown by the physical vapor

transport method [9]. After purifying crude powder samples supplied from Nipponkayaku Company by vaporizing at 285 °C and coarse crystallization at 213 °C in a two-zone tube furnace under Ar gas flow, the coarse crystals are slowly recrystallized at the same temperature in approximately three days.

The electric transport measurements are performed by the four-terminal technique at room temperature, so that extrinsic pressure dependence at electric contacts between the semiconductors and metal electrodes is excluded. All the components of the samples are fabricated by polymer materials except for gold electrodes in order to realize nearly homogeneous shrinkage under the applied pressure. The field-effect transistor (FET) samples with the top-contact and bottom-gate structure are fabricated as follows. A patterned gate electrode of 20 nm thickness is first vapor deposited through a shadow mask on a polyethylene naphthalete (PEN) substrate. A gate-insulating layer of CYTOP (Asahi Glass Company) is formed by spin coating and subsequent heat treatment at 140 °C for 15 h. A single-crystal DNTT flake with a thickness of less than 1 μm is carefully taken and laminated on the position of the gate electrode. A photograph of typical single crystal DNTT platelet employed in this study is shown in Fig. 1. Source-drain electrodes and four voltage terminals are constructed by vapor deposition of 2, 3, 5, 6-tetrafluoro-7, 7, 8, 8-tetracyanoquinodimethane and over-deposited gold layers through a shadow mask to the thickness of 1 and 20 nm, respectively. Carbon paste is laid on the electrodes at the edges of the DNTT flake to repair electric disconnection. Finally, the Hall-bar-shaped channel is fabricated with the use of laser etching equipment so that the central channel is structured on the gate electrode. The width and length of the channel are 100 and 150 μm, respectively. The distance between adjacent voltage terminals along the channel direction is 50 μm. The device is covered with a few-μm thick parylene for passivation and then completely filled in epoxy (STYCAST 1266) for the mechanical stability. The whole piece is introduced in a standard Cu-Be pressure cell and Fluorinert FC70/77 is used for the pressurizing medium.

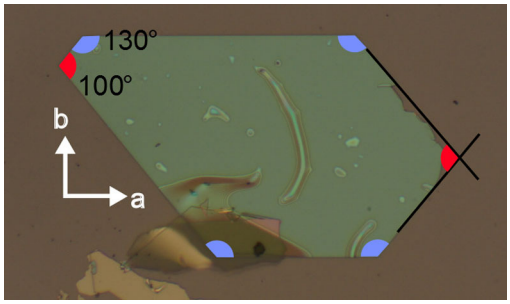

FIG. 1 (color online). A photograph of a single crystal platelet of DNTT. Angles marked by black (red) and gray (blue) symbols are 100° and 130°, respectively. Crystalline directions for the a and b axes are indicated by white arrows.

In the present Letter, we mainly discuss pressure dependence of the four-terminal carrier mobility $\mu(P)$ to quantitatively argue the pressure effect of the charge transport excluding influence of the parasitic contact. μ is defined as

$$\mu = \frac{1}{C}\frac{\partial\sigma}{\partial V_G}, \tag{1}$$

where C is the capacitance of the CYTOP gate insulator in a unit area, σ is the four-terminal sheet conductivity and V_G is the applied gate voltage. Since C is varied with the applied pressure, we use the value of modified C as a function of pressure which was identified in our previous study; we estimated V_G dependent carrier density under each pressure by precise Hall-effect measurements using rubrene single-crystal FETs, so that $C(P)$ turned out to change by 10% at 0.5 GPa [6]. μ is estimated at $V_G = -100$ V, where field-induced carriers are accumulated at the bottom of the conduction band to avoid confusion due to the trap-involved pressure effect in the subthreshold region such as we encountered for rubrene single-crystal transistors [6].

In order to have an idea of the deformed unit cells under a pressurized condition, x-ray diffraction experiments were carried out using well-purified DNTT powder samples by a synchrotron radiation source on the beam line BL10XU at SPring-8. The sample is introduced into a diamond anvil cell with the pressure medium (Fluorinert, FC70/77). Applied pressure is determined by a simultaneous ruby fluorescence measurement. The wavelength of the x-ray was 0.41413 Å. The diffraction patterns were obtained with an imaging plate detector as a function of 2θ (θ is an incident angle of x-ray). The structural change extracted from the powder x-ray diffraction experiment gives a guide to the deformed molecular packing in the transistor devices, though it is influenced by the deformation of the substrates. To minimize the effect, we use plastic substrates with similar thermal contraction rate as organic semiconductors.

The unit cell of DNTT is monoclinic, so that there are four parameters of three lattice constants along the a, b, and c axes and an angle β. The x-ray diffraction (XRD) patterns as a function of 2θ show no disappearance or emergence of peaks with increasing pressure, indicating that there is no structural phase transition up to about 2 GPa [10]. It can be noticed that every peak shifts toward a larger angle, which indicates overall shrinkage of the unit cell. We choose four distinctive peaks assigned to (100), (003), (020), and $(11\bar{1})$ to identify the four structural parameters. We note that the result is consistent with the positions of all other visible peaks [10].

Plotted in Figs. 2(a) and 2(b) are the variation of these parameters as a function of pressure. It turned out that the lattice constants along the a and c axes and β show drastic change at the pressure approximately lower than 0.2 GPa and that they vary with a much slower rate at higher

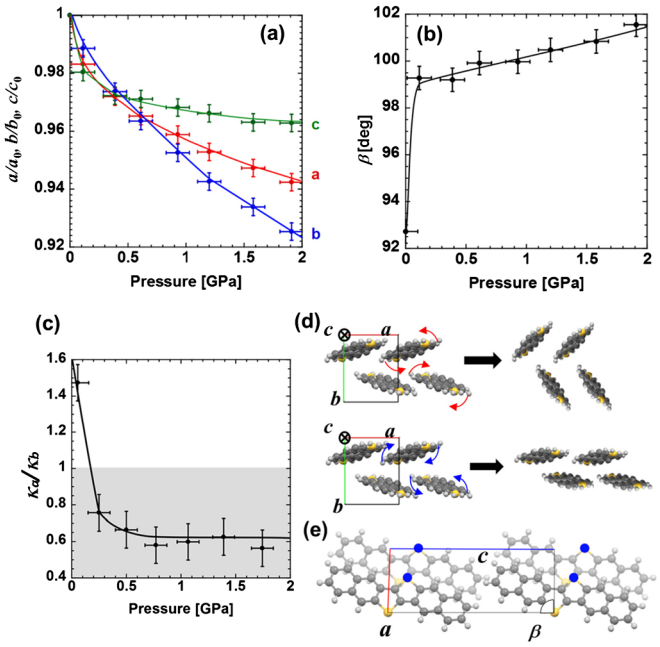

FIG. 2 (color online). Pressure dependence of (a) lattice constants for three axes and (b) β as the intersection angle between the a and c axes. (c) Ratio of compressibility between the a and b axes as a function of applied pressure. (d) Two suggested molecular arrangements in cases of shrinkage along the a axis (above) and b axis (below), respectively. Curved arrows indicate the direction of molecular rotation. (e) Crystal structure viewed perpendicular to ac plane. Dark and light molecular images indicate molecules located on the front and back sides, respectively.

pressures, whereas the constant along the b axis is varied with an almost constant rate. Furthermore, in order to give an idea of molecular rearrangement under pressure, we plot the ratio of compressibility $\kappa_a(= da/dP)$ and $\kappa_a(= db/dP)$ in Fig. 2(c). Here the compressibility is defined as the differential coefficient estimated from two adjacent points in Fig. S2 in the Supplemental Material [10],

$$\kappa(P) = \frac{1}{L(P_i)} \frac{L(P_i) - L(P_j)}{P_i - P_j}, \tag{2}$$

where P_i and P_j are two adjacent pressure for the plot in the Supplemental Material [10], Fig. S1 ($P_i > P_j$). $L(P_i)$ and $L(P_j)$ are the lattice constants evaluated at each pressurized condition. Thereby, anisotropic lattice parameters and compressibility at each pressure, which describes the tendency to deform in each direction, are given in Figs. 2(a) and 2(c) for further discussion.

Since the ratio is larger than 1 ($\kappa_a/\kappa_b > 1$) below approximately 0.2 GPa, the tendency to restrict in the a direction is major in this region, so that molecules are supposed to be rearranged with concomitant rotation indicated by the curved red arrows as illustrated in Fig. 2(d). On the other hand, the unit cell starts to shrink more drastically in the b axis direction so that $\kappa_a/\kappa_b < 1$, in which one can assume molecular rotation in the opposite direction as indicated by curved blue arrows in Fig. 2(d). The relationship between dominant compressive direction and the corresponding molecular rearrangement given here is consistent with the structural change observed in oligoacene systems such as anthracene, pentacene, and tetracene under high pressure [11,12]. We emphasize that such nonmonotonic evolution of κ_a/κ_b as the result of the on-site rotation is generated by the specific molecule-to-molecule interaction due to the peculiar shape of the molecular orbital, in sharp contrast to the case of inorganic semiconductors which consists of more symmetric atoms. Since the predominant direction of the differential compression is of weaker intermolecular interaction, the observation indicates that the balance of the interaction has changed with increasing pressure. It is suspected that the distance between the two molecules in the b direction becomes too narrow to further shrink after the rotation depicted in the upper panel in Fig. 2(d) at the beginning, causing the molecular rotation in the reverse direction with further application of the pressure.

Noting that the pressure dependence of the dimension along the c axis and β looks similar, we further discuss the molecular dislocation in the ac plane to understand the observation. Considering the crystal structure in the ac plane shown in Fig. 2(e) the increase in the angle β and shrinkage in c look both to have originated from displacement of neighborhood molecules on the a direction, presumably because of considerable density of the electron distribution at the sulfur atoms. The π electrons tend to be further distributed at electronegative sulfur atoms as compared with carbon and hydrogen sites [13], in addition to the effect of spatially large occupation of the $3p_z$ orbitals in the sulfur atoms. As the interaction between nearest-neighbor sulfur atoms marked by blue circles in Fig. 2(e) becomes large with increasing pressure, the adjacent molecules tend to displace in the c direction to minimize the energy cost for Coulomb repulsion. Since the sulfur-to-sulfur interaction is pronounced in the a-axis direction, both the c and β parameters change drastically under relatively low pressure in the region of $\kappa_a/\kappa_b > 1$, while the values are less sensitive to pressure when the shrinkage in the b direction becomes dominant at higher pressures. The predominance of the sulfur-to-sulfur interaction in the a direction also results in significantly higher mobility in the a direction as compared to that in the b direction, which is linked to a considerable portion of the transfer integral due to the sulfur-to-sulfur interaction. Note that the change in β up to 10° is a contrasting result to those in sulfur-free oligoacene systems in which there are only a few degrees of deviation before and after pressurization for angles, so called α, β, and γ [11,12].

Pressure effects on the mobility of carriers in DNTT-FETs are measured in both the a and b axes preparing devices

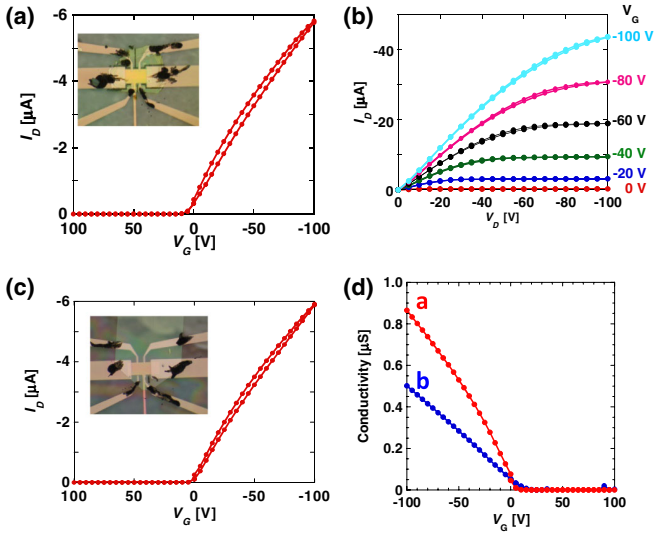

FIG. 3 (color online). (a) Transport and (b) output properties of DNTT-FET for the a-axis conducting direction. (c) Transport properties of DNTT-FET for the b-axis conducting direction. Pictures for each device are inserted in (a) and (c). (d) Four-terminal conductivity along the a and b axes at ambient condition. The estimated carrier mobility is 2.1 $\mathrm{cm}^2/\mathrm{V\,s}$ for the a axis and 1.3 $\mathrm{cm}^2/\mathrm{V\,s}$ for the b axis at $V_G = -100$ V, respectively.

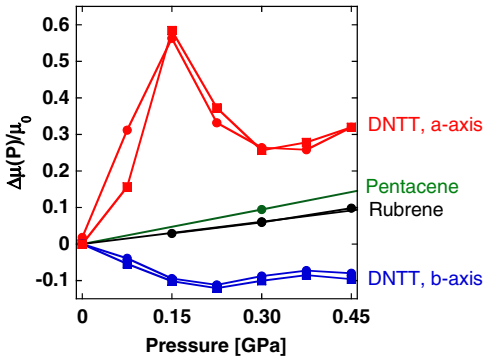

FIG. 4 (color online). Pressure effect on DNTT-FET for the a and b axes. Those for pentacene and rubrene devices are also plotted for comparison. Circles and squares indicate the data obtained while in the compression and decompression processes, respectively.

similarly whose transport and output properties and gate-voltage dependence of carrier conductivity are shown in Fig. 3. The increasing rate of the mobility is defined as $[\mu(P) - \mu(0)]/\mu(P) = \Delta\mu(P)/\mu(P)$, where $\mu(P)$ and $\mu(0)$ are the four-terminal mobility at the pressure P and in the ambient condition. Note that estimated carrier mobility along each axis in ambient condition is 2.1 $\mathrm{cm}^2/\mathrm{V\,s}$ for the a axis and 1.3 $\mathrm{cm}^2/\mathrm{V\,s}$ for the b axis, respectively, and this anisotropic behavior is in agreement with our previous report [14]. The pressure dependence of μ is exhibited in Fig. 4 at the drain bias voltage V_D of -10 V. It is confirmed that μ follows the same curvature reversibly against compression and consecutive decompression processes. As plotted with the pressure dependent mobility for rubrene [6] and pentacene devices [15], the pressure dependence is much more drastic for DNTT-FETs in size and in the nonmonotonic features. In particular, the a-axis device shows a peak structure at 0.15 GPa in contrast to other two organic FETs exhibiting simple linear responses.

The peak feature in Fig. 4 is to be consistently understood with the result in Fig. 2(c). The peak profiles of $\Delta\mu(P)/\mu(P)$ indicate that the derivative $d\mu/dP$ changes the sign at 0.15 GPa for the a axis, which is in coincidence with the crossover point of $\kappa_a/\kappa_b = 1$, representing a change in the nature of the anisotropic deformation at the same pressure. Therefore, the anomalous behavior of the carrier mobility against pressure on DNTT-FET appears to be highly linked to the molecular rearrangement described above based on the structural data. When $P < 0.15$ GPa, the structural analysis suggested that the molecules tend to rotate so that face-to-face π-π stacking is enhanced along the a axis, causing a significant increase in μ_a and decrease in μ_b. On the other hand, upon pressurizing above 0.15 GPa, the structural change influences oppositely, so that μ_a significantly decreases and μ_b slightly increases. Therefore, the peak structure results from crossover between the two distinct molecular rotations associated with pressurization. We note that the x-ray structural analysis is based on the samples without substrates, meaning that the above comparison is not fully precise with finite error bars for the crossover point. Though the substrates of similar compressibility as organic crystals can cause discrepancy from the situation plotted in Fig. 2(a) because of more isotropic restriction, the result of the pressure dependent mobility indicates that the direction of the on-site molecular rotation is governed by the compressibility ratio at each pressure point, which is approximated by the structural data without substrates.

At the pressure higher than 0.30 GPa, μ_a slightly increases simply due to predominance of the normal pressure effect due to increased density of the molecules. The effect of the on-site molecular rearrangement is not pronounced any longer in this region. We also note that the peak feature itself was observed in rubrene single-crystal FETs at much higher pressure above 0.60 GPa, but the effect turned out to be due to the disordering of crystal structure coming from the presence of the phenyl group on the periphery of central tetracene structure as the result of detailed structural studies [16]. For further elucidation of the structure-property relations of pressure-sensitive organic semiconductors, crystal structure analysis under pressurization should be completed in the future so that we complement the detailed information about the molecular rearrangement.

As for quantitative consideration of the size of the pressure coefficient for the carrier mobility, the value of 3.8 GPa^{-1} in the a direction for the present DNTT-FET is extremely large below 0.15 GPa, as compared to those for rubrene and pentacene, which is already 1 order larger than typical values for inorganic materials [17]. In conjunction

with the significant contribution of the sulfur-to-sulfur interaction, which causes peculiar displacement in the ac plane, the presence of sulfur atoms in DNTT molecules is responsible for the anomalous pressure dependence in μ, indicating the significant contribution of the $3p_z$ orbitals on sulfur to the charge transport in the semiconductors and to the device performances.

In conclusion, DNTT was found to exhibit an anomalous pressure effect in both its crystal structure and electric transport. Through this study, in addition to degrees of freedom in the relative arrangement of the adjacent molecules, it is clarified that the presence of sulfur atoms governs the pressure response of DNTT. The access to nearest-neighbor sulfur atoms as a result of pressurization leads to the drastic deformation and the simultaneous molecular rearrangement in order to suppress the repulsive interaction between negatively charged sulfur atoms. And the corresponding pressure effect of carrier transport on DNTT-FETs can be well explained by considering with the structural change, indicating the successful observation of the so-called structure-property relations. Furthermore, an extremely large pressure response up to 3.8 GPa^{-1} is attributed to the widely spread $3p_z$ orbital localized on the sulfur atom. These experimental results can be good evidence of how the heteroatom influences the properties of heteroacene-based molecular solids.

This work is financially supported by Grant-in-Aid for Scientific Research (Grant No. 22245032 and No. 236860050) from MEXT in Japan. We thank Nippon Kayaku Corporation for supplying organic semiconductor DNTT used in the present experiments.

*ksakai@sanken.osaka-u.ac.jp
†takeya@sanken.osaka-u.ac.jp

[1] J. Takeya, K. Tsukagoshi, Y. Aoyagi, T. Takenobu, and Y. Iwasa, Jpn. J. Appl. Phys. **44**, L1393 (2005).
[2] V. Podzorov, E. Menard, J. A. Rogers, and M. E. Gershenson, Phys. Rev. Lett. **95**, 226601 (2005).
[3] J. Takeya, J. Kato, K. Hara, M. Yamagishi, R. Hirahara, K. Yamada, Y. Nakazawa, S. Ikehata, K. Tsukagoshi, Y. Aoyagi, T. Takenobu, and Y. Iwasa, Phys. Rev. Lett. **98**, 196804 (2007).
[4] M. Yamagishi, J. Soeda, T. Uemura, Y. Okada, Y. Takatsuki, T. Nishikara, Y. Nakazawa, I. Doi, K. Takimiya, and J. Takeya, Phys. Rev. B **81**, 161306(R) (2010).
[5] T. Uemura, M. Yamagishi, J. Soeda, Y. Takatsuki, Y. Okada, Y. Nakazawa, and J. Takeya, Phys. Rev. B **85**, 035313 (2012).
[6] Y. Okada, K. Sakai, T. Uemura, Y. Nakazawa, and J. Takeya, Phys. Rev. B **84**, 245308 (2011).
[7] Z. Rang, M. I. Nathan, P. P. Ruden, V. Podzorov, M. E. Gershenson, C. R. Newman, and C. Daniel Frisbie, Appl. Phys. Lett. **86**, 123501 (2005).
[8] Z. Rang, M. I. Nathan, P. P. Ruden, R. Chesterfield, and C. Daniel Frisbie, Appl. Phys. Lett. **85**, 5760 (2004).
[9] Ch. Kloc, P. G. Simpkins, T. Siegrist, and R. A. Laudise, J. Cryst. Growth **182**, 416 (1997).
[10] See Supplemental Material at http://link.aps.org/supplemental/10.1103/PhysRevLett.110.096603 for the x-ray diffraction pattern of DNTT powder under pressurization.
[11] M. Oehzelt, R. Resel, and A. Nakayama, Phys. Rev. B **66**, 174104 (2002).
[12] M. Oehzelt, A. Aichholzer, R. Resel, G. Heimel, E. Venuti, and R. G. Della Valle, Phys. Rev. B **74**, 104106 (2006).
[13] R. S. Sanchez-Carrera, S. Atahan, J. Schrier, and A. Aspuru-Guzik, J. Phys. Chem. C **114**, 2334 (2010).
[14] M. Uno, Y. Tominari, M. Yamagishi, I. Doi, E. Miyazaki, K. Takimiya, and J. Takeya, Appl. Phys. Lett. **94**, 223308 (2009).
[15] K. Sakai, Y. Okada, S. Kitaoka, T. Uemura, Y. Ohishi, A. Fujiwara, and J. Takeya (unpublished).
[16] A. R. Hutson, A. Jayaraman, and A. S. Coriell, Phys. Rev. **155**, 786 (1967).
[17] Y. Okada, K. Sakai, S. Kitaoka, T. Uemura, Y. Ohishi, A. Fujiwara, and J. Takeya (unpublished).